Mapping of Corneal Layer Thicknesses With Polarization-Sensitive Optical Coherence Tomography Using a Conical Scan Pattern

Florian Beer,[1,2] Andreas Wartak,[1] Niklas Pircher,[3] Stephan Holzer,[3] Jan Lammer,[3] Gerald Schmidinger,[3] Bernhard Baumann,[1] Michael Pircher,[1] and Christoph K. Hitzenberger[1]

[1]Center for Medical Physics and Biomedical Engineering, Medical University of Vienna, Vienna, Austria
[2]Institute of Applied Physics, Vienna University of Technology, Vienna, Austria
[3]Department of Ophthalmology and Optometry, Medical University of Vienna, Vienna, Austria

Correspondence: Florian Beer, Center for Medical Physics and Biomedical Engineering, Medical University of Vienna, Währinger Gürtel 18-20, 4L A-1090 Vienna, Austria; florian.beer@meduniwien.ac.at.

Submitted: July 17, 2018
Accepted: October 18, 2018

Citation: Beer F, Wartak A, Pircher N, et al. Mapping of corneal layer thicknesses with polarization-sensitive optical coherence tomography using a conical scan pattern. *Invest Ophthalmol Vis Sci*. 2018;59:5579–5588. https://doi.org/10.1167/iovs.18-25311

Purpose. We demonstrate segmentation and mapping of corneal layers (epithelium, Bowman's layer, and stroma) across the entire cornea (limbus to limbus), using additional contrast provided by polarization-sensitive optical coherence tomography (PS-OCT) and analyze the reproducibility of the procedure.

Methods. A custom built PS-OCT system operating at 1045 nm central wavelength with conical scanning was used for image acquisition. Conical scanning allows for almost perpendicular beam incidence on the corneal surface and provides good signal quality over the entire field of view. Epithelium, Bowman's layer, and stroma were segmented using the additional contrast provided by PS-OCT. Thickness maps were computed and analyzed in sectors. Both eyes of 20 healthy volunteers were imaged at least three times to test this method and to quantify reproducibility.

Results. Thickness maps of the epithelium show significant ($P < 0.001$) superior thinning and an inferior thickening. Bowman's layer appears homogeneous within the central 7 to 8 mm diameter of the cornea and gets thinner toward the periphery until this layer disappears between 4 and 5.5 mm eccentricity from the center. Intersubject variations of the measured thicknesses of epithelium (coefficient of variation [CV] ∼8%), Bowman's layer (CV∼25%), and stroma (CV∼10%) were observed. Very good reproducibility of thickness measurements of epithelium (CV < 3%), Bowman's layer (CV < 5%), and stroma (CV < 2%) was found. Furthermore, a significant correlation ($P < 0.001$) between layer thicknesses of the right and left eyes of the same subject was found.

Conclusions. PS-OCT with conical scanning is a feasible approach for determining thickness maps of corneal layers on a large field of view with high reproducibility.

Keywords: optical coherence tomography, polarization-sensitive imaging, cornea, corneal epithelium, Bowman's layer

The human cornea has a layered structure that has been studied extensively by histology and various imaging modalities and is well known today.[1,2] The outmost layer, the corneal epithelium, is 4 to 6 cell layers thick (40–50 µm)[1] and is separated from the stroma by Bowman's layer, which is a smooth acellular layer composed of randomly oriented collagen fibrils and has an average thickness of 15 µm.[2] The stroma consists of approximately 200 stacked lamellae, each composed of highly organized parallel collagen fibrils.[2]

Several methods have been developed and demonstrated for performing such measurements, such as confocal microscopy,[3] high-frequency ultrasound,[4,5] and, most recently, optical coherence tomography (OCT).[6] OCT is a noninvasive, noncontact imaging technique that provides high image resolution, operates at high imaging speeds, and has meanwhile become a standard clinical tool in ophthalmology.[7–9] First applications to measure corneal thickness by low coherence interferometry, the basic ranging technique of OCT, were reported as early as 1992,[10,11] where measurement precisions down to 1.5 µm could be demonstrated in vivo. Meanwhile, measurement of corneal thickness by anterior segment OCT is a standard procedure.[6]

For more detailed studies on corneal diseases, measurement and imaging of individual corneal layers is required. Epithelial thickness (ET) measurements were described by various studies using custom built OCT[12,13] or commercial[14,15] devices. Most of these studies report an ET between 50 and 60 µm measured in a field of view (FoV) of up to 9 mm diameter. Only few studies report on mapping of Bowman's layer thickness (BLT), all of them using ultra-high resolution (UHR) OCT.[13,16–18] These studies reported thickness values of 15 to 20 µm. The stromal thickness (ST) accounts for approximately 90% of the corneal thickness and has been studied and described in the literature.[2,5] At its thinnest point near the corneal apex, the corneal stroma is 460 to 530 µm thick and shows a radial increase in thickness toward the periphery.[2,19]

Various corneal diseases lead to alterations of this regular structure and manifest themselves in thickness changes of these

layers. Therefore, a considerable interest in rapid and precise in vivo imaging and measurement of these layers exists.

Current approaches to measure and map the thickness of corneal layers suffer from two shortcomings. First, imaging of the cornea is limited to a small FoV when using regular telecentric scanning (parallel probing beams) because of the reduction of signal intensity and axial resolution in paracentral regions due to the large inclination of the incident beam to the corneal surface.[20] To overcome this problem, we recently introduced a conical scan pattern that provides almost perpendicular incident angles on the corneal surface, which maintains signal intensity and axial resolution over the entire FoV (11 mm diameter).[21]

Second, conventional OCT suffers from limited contrast of intensity-based images. Especially, segmentation of Bowman's layer is quite difficult because its boundary to the stroma frequently suffers from poor image contrast. To overcome this problem, polarization sensitive (PS) OCT can be used. PS-OCT is a functional extension of OCT that enables detection of tissue-specific polarization changes of the probing light and, therefore, provides additional contrast.[22,23] When imaging the cornea with PS-OCT, epithelium and Bowman's layer show polarization-preserving properties; therefore, the polarization state of the probing beam backscattered by the epithelium or Bowman's layer remains unchanged.[21] The corneal stroma has previously been analyzed in detail by PS-OCT.[21,24] It is known to be birefringent, whereby the collagen lamellae of which the stroma consists generate a characteristic retardation pattern in the probing light beam that depends on the angle of incidence on the corneal surface.[24] If a telecentric scan pattern is used, the retardation is low near the corneal center (at perpendicular incidence) and increases—with the increasing inclination to the corneal surface—toward the periphery. This regular retardation pattern can be heavily distorted by diseases, such as keratoconus.[25,26] Using the conical scan pattern, this surface angle–dependent retardation is largely eliminated, and a residual retardation pattern caused by the birefringence of preferentially aligned, reinforcing collagen fibers is observed.[21]

While the stromal birefringence affects the transmitted light, it is important to note that light directly backscattered by the stroma has a strong depolarized component.[21,27] This effect can be used to identify stromal tissue and to segment the boundary between Bowman's layer and the stroma, an effect that is exploited—to the best of our knowledge for the first time—in this study.

We demonstrated segmentation and mapping of the thicknesses of epithelium, Bowman's layer, and stroma in the eyes of healthy subjects. To overcome the limitations of telecentric scanning and limited intensity contrast, PS-OCT was combined with conical scanning and used for imaging. The additional contrast provided by PS-OCT and the high signal-to-noise ratio (SNR) over the entire FoV enables the segmentation of corneal layer boundaries and the calculation of three-dimensional thickness maps. The results were compared to values found in the literature and the reproducibility of our measurements was analyzed.

Methods

PS-OCT Scanning

A custom built, single-mode fiber based swept-source PS-OCT prototype operating at a central wavelength of 1045 nm with a spectral bandwidth of 100 nm was used for imaging.[21,28] The system uses a specially-designed scanning optics containing an aspheric condenser lens to enable conical scanning, which allows for almost perpendicular beam incidence on the corneal surface and provides good signal quality over the entire FoV (limbus-to-limbus) compared to the standard telecentric scanning approach (Fig. 1).[21] The lateral resolution given by the focusing optics is approximately 33 μm ($1/e^2$ beam focus diameter) at the center and decreases to 40 μm at the outmost periphery of the FoV. The axial resolution of the instrument is 6.3 μm in corneal tissue (assuming a group refractive index of 1.385). Operating at 100 kHz A-scan rate and using a raster scan pattern, one volume consisting of 150 B-scans with 1024 A-scans per B-scan is acquired in <2 seconds. The incident power of the probe beam onto the cornea was set to 1.8 mW, which is well below the maximum permissible exposure for this wavelength as specified by the International Electrotechnical Commission safety standard IEC 60825-1.[29]

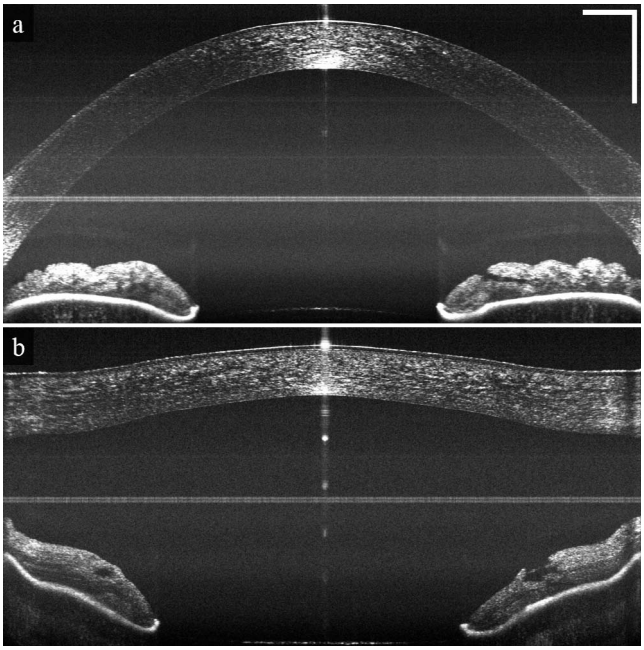

Figure 1. Representative central B-scan (10 times averaged) using (**a**) telecentric scanning and (**b**) conical scanning. Conical scanning improves the signal in peripheral areas; however, leads to a distorted corneal shape.[21] *Scale bars*: 1 mm in lateral and axial direction.

For polarization sensitive imaging, the sample is illuminated by a single, circular polarization state, and the detected light is analyzed in two orthogonal polarization channels. The co-polarized channel shows polarization-preserving structures, such as epithelium, Bowman's layer, and the endothelium, as well as the co-polarized light components backscattered by the stroma (Fig. 2a). The cross-polarized channel on the other hand shows cross-polarized light components, essentially generated by depolarizing and birefringent structures in the stroma (Fig. 2b). The differences in the two channels can be seen clearly in the color coded (co-polarized channel: red, cross-polarized channel: green) superposition of the two channels.

Segmentation of Corneal Layers

After standard preprocessing of the recorded spectral data, strong specular reflections were observed in the B-scans and removed via intensity thresholding before further processing for corneal layer segmentation. As the epithelium, top surface of Bowman's layer, and endothelium are mainly visible in the image data of the co-polarized channel, the segmentation of these layers was performed solely on these images. In a first step, the B-scan images were smoothed (floating average of 10 pixels in lateral direction) and the anterior surface of the

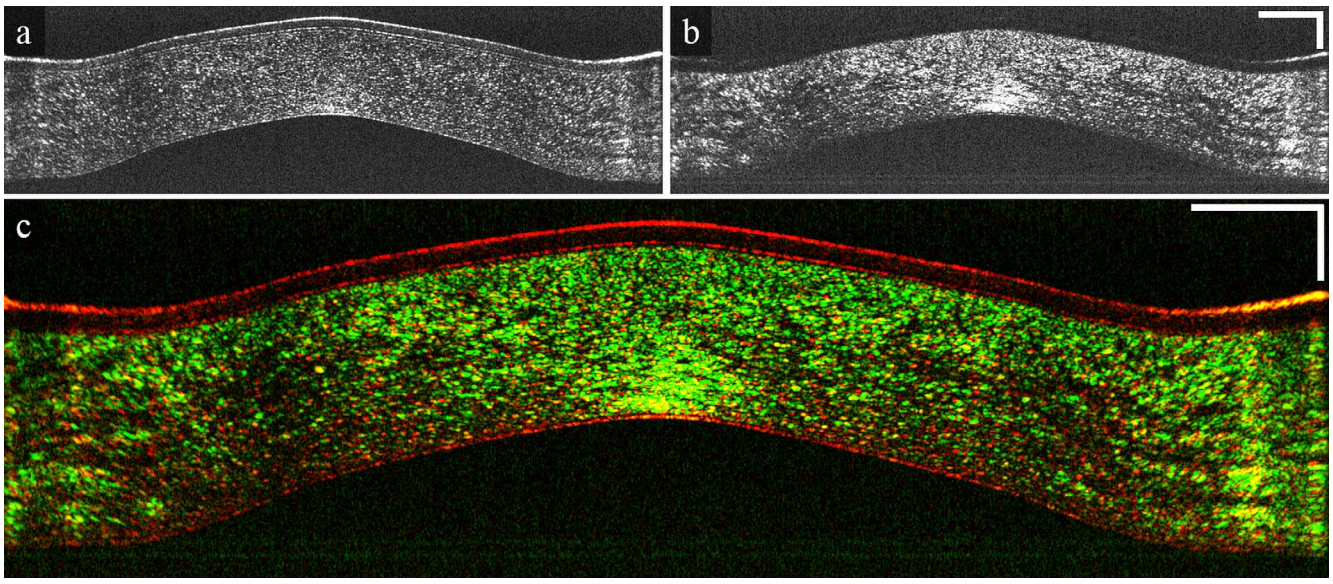

FIGURE 2. (**a**) Co- and (**b**) cross-polarized channel of a representative corneal B-scan and (**c**) the color-coded superposition of the two channels (co-polarized channel: *red*, cross-polarized channel: *green*). *Scale bars*: 1 mm in lateral direction and 200 µm in axial direction.

cornea was detected in the resulting image using a peak detector (detection of the first peak along an A-scan). Outliers were removed, and the remaining surface points were interpolated with a cubic spline, to obtain a homogeneous and smooth surface. The result of this detection procedure can be seen in Figure 3a. The B-scan images were flattened along the detected surface by removing pixels anterior to the surface of the cornea and by image cropping as seen in Figure 3b. Due to the almost perpendicular incidence angles of the probing beam on the corneal surface provided by the conical scanning, distortion of deeper layers caused by refraction at the surface can be neglected.[21] Thus, no refraction correction of the image data was performed.

In a next step, the entire flattened 3D volume was smoothed in both lateral directions by applying a floating average window of 15 (A-scans) × 5 (B-scans) pixels. The window size was determined empirically and yielded the visually best segmentation results. The posterior surface of the cornea was segmented by using the same procedure as used for the anterior corneal surface (peak detection, removing of outliers, spline interpolation). In this case, the first peak along the A-scan in reverse direction, starting from the anterior chamber, is detected, providing the back-surface of the cornea (Fig. 3b). The interface between epithelium and Bowman's layer was segmented by finding the first peak along the A-scan direction starting from the corneal surface (Fig. 3c). Lastly, the posterior surface of Bowman's layer (which is equal to the anterior surface of the stroma) was segmented using the information of the cross-polarized channel. The light backscattered by the stroma is highly depolarized. Thus, the surface of the stroma can be easily detected in the images of the cross-polarized channel by using a thresholding algorithm (the first point above a manually set intensity threshold is detected). Similar as above, outliers are removed, and a cubic spline was fitted to the detected points. The segmentation result is displayed in Figure 3d. Figure 3e shows all segmented surfaces in red overlaid on the polarization independent image (sum of the squares of both co- and cross-polarized channel—from here on referred to as intensity). The individual thresholds for detection of each interface in each eye were chosen empirically to compensate for differences in image quality and were set according to the visually best segmentation results. Apart from setting the thresholds, the segmentation was performed automatically.

To generate en face maps of the interfaces of each layer, the segmentation was done for all B-scans of the volume. By subtracting the segmented interfaces from each other, maps of ET, BLT, ST, and total corneal thickness (CT) were retrieved. To remove segmentation errors, these maps were smoothed by applying a floating average filter with a window size of 10 pixels (A-scans) × 3 pixels (B-scan).

For further analysis, these maps were divided in 25 sectors and are illustrated in Figure 4. All data points contained in one sector were averaged to enable localized comparison of layer thicknesses and to test the reproducibility of the thickness measurements. Sectors 15, 16, 19, 20, 23, and 24 were excluded from the analysis because eyelid and eyelashes were obstructing large parts of this region and prohibited reliable measurement results in these areas. Additionally, sectors equidistant to the corneal apex were combined into three concentric rings (first ring, sectors 1–8; second ring, sectors 9–14; and third ring, sectors 17, 18, 21, and 22) for reproducibility and correlation analysis. To evaluate nasal and temporal characteristics for left and right eyes, the corresponding sectors were mirrored along the vertical axis (superior to inferior) through the center of the cornea.

Statistical Analysis

All layer thickness values are given in micrometers as mean ± SD and are converted from optical to geometrical thickness assuming a group refractive index of 1.385. The SD in all cases (apart from reproducibility measurements) reflects the variability among subjects. A Kolmogorov-Smirnov test was performed on the data and showed normal distribution. For analyzing the reproducibility of thickness measurements, SD and coefficient of variation (CV) between consecutive measurements were calculated for each layer. To analyze the significance of ET changes in nasal–temporal and superior–inferior directions and for analyzing the significance of radial changes in BLT a 2-tailed, paired *t*-test was performed. For

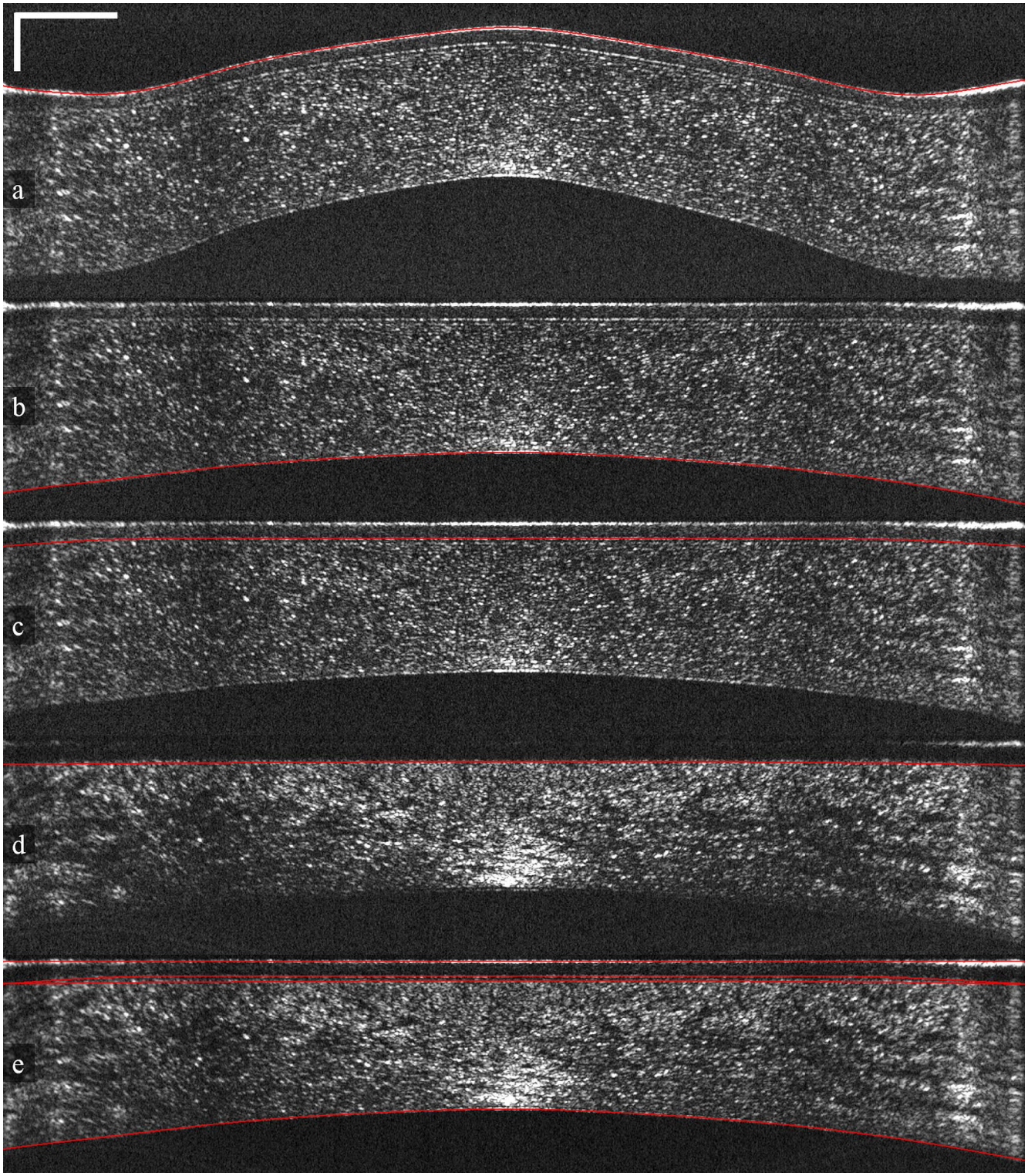

FIGURE 3. Representative images of the cornea of a healthy volunteer showing the different steps of the segmentation and flattening procedures. Segmented interfaces shown as *red lines*. (**a**) Anterior epithelial surface (co-polarized channel), (**b**) endothelial surface after flattening (co-polarized channel), and (**c**) posterior epithelial surface (co-polarized channel). (**d**) Anterior stromal surface detected in the cross-polarized channel. (**e**) Visualization of all segmentation lines superimposed onto the intensity image. *Scale bars*: 1 mm in lateral direction and 200 µm in axial direction (all images are displayed on a logarithmic gray scale).

comparison of thickness values between right and left eyes, Pearson's correlation coefficient r and the corresponding P value were calculated for the central sector and three consecutive concentric rings (combining sectors equidistant to the corneal apex) for all layers in the 20 eye pairs. Correlation between layers was analyzed by calculating Pearson's correlation coefficient r and the corresponding P value for the central sector and the three concentric rings.

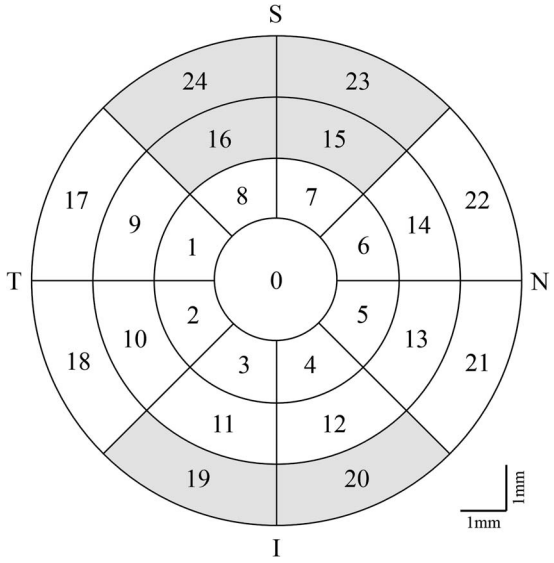

Figure 4. Scheme of the arrangement of sectors for quantitative evaluation of the layer thicknesses: Central sector (0) lies within a 1.3 mm radius. Concentric rings with 1.3 mm width are divided into eight subsectors each. Sectors marked in *gray* (15, 16, 19, 20, 23, and 24) were not considered for evaluation as the signal was partially obstructed at these locations due to shadowing by eyelid and eyelashes.

Study Population

Both eyes of 20 healthy volunteers (all Caucasian, 12 men and 8 women; mean age, 33 ± 6 years; age range, 25–49 years) were measured for this study. Each eye was measured three to five times in one imaging session (5–10 minutes) for reproducibility analysis. To simulate independent measurement sessions the subject was asked to sit back, and the headrest was intentionally misaligned and realigned between individual measurements. The study was approved by the ethics committee of the Medical University of Vienna and followed the tenets of the Declaration of Helsinki. Informed consent was obtained from all volunteers before measurement.

Results

Thicknesses of Corneal Layers

Maps of ET, BLT, ST, and CT of all measured eyes were computed and analyzed in sectors. Figure 5 shows representative maps of the right eye of a healthy volunteer with the sector-map superimposed. Evaluation of the averaged (over the study group) thicknesses per sector for right and left eyes is displayed in Figure 6. The error bars indicate the variation among subjects.

Mean ET of the central sector was 54.1 ± 2.8 μm and showed a decrease of 2.7 ± 2.7 μm per ring in superior direction and an increase of 1.7 ± 0.9 μm per ring in inferior direction. The thickness change in vertical direction was significant ($P < 0.001$). Additionally, ET was on average 1.3 ± 3.5 μm thinner in the peripheral sectors in the nasal direction than on the temporal side, which was not significant ($P = 0.48$). Bowman's layer showed an almost uniform thickness of 15.4 ± 2.4 μm in the central sector and 15.4 ± 2.5 μm in the first ring. Followed by a slight increase in thickness to 16.5 ± 3.2 μm in the second ring, which was insignificant ($P = 0.05$), a significant thinning toward the periphery ($P < 0.001$) to an averaged thickness of 13.4 ± 5.9 μm in the third ring was found. An averaged central ST of 498.9 ± 36.1 μm was measured which increased steadily toward the corneal periphery. It showed a larger increase in thickness in the inferior than in the superior direction. Figure 7 shows the contribution of the central thickness of individual layers to the CT. Being the thickest layer, the corneal stroma clearly is the main contributor to variations in CT.

Table 1. Summary of the Reproducibility Measurements: Average SD and CV of the Central Sector and of Three Concentric Rings of All Consecutive Measurements of 40 Eyes

	Reproducibility of Consecutive Measurements			
	ET	**BLT**	**ST**	**CT**
Center				
SD, μm	0.5	0.3	1.0	1.1
CV, %	0.9	1.7	0.2	0.2
First ring				
SD, μm	0.9	0.5	5.9	6.9
CV, %	1.8	3.4	1.1	1.2
Second ring				
SD, μm	1.0	1.2	8.6	9.6
CV, %	1.9	7.0	1.5	1.5
Third ring				
SD, μm	2.5	2.4	17.4	19.6
CV, %	4.6	19.0	3.0	3.0

Reproducibility

To demonstrate the reproducibility of our technique, all eyes were measured three to four consecutive times and the SD of these consecutive measurements was calculated for all layers and sectors. Figure 8 shows the mean thickness of each sector for all layers of one representative eye measured four consecutive times. The error bars indicate the SD between consecutive measurements.

The SD of individual layer thicknesses between consecutive measurements was calculated for each sector and layer for each individual subject. The layer thicknesses and SD values were averaged over all 40 eyes for the central sector and the three concentric rings to calculate the corresponding CV value (Table 1). The calculated SD values indicated a very good reproducibility of corneal layer thickness measurements using our method, especially for the central area.

Layer Correlations

In addition, we compared layer thicknesses measured in right and left eyes of the same individual and found very strong correlation for the central sector, decreasing toward the periphery (Table 2). Figure 9 shows the correlation between right and left eyes for the central sector in a Bland-Altman plot. In a final step we investigated if thicknesses of individual layers were correlated. We found that only ST and CT showed a strong significant correlation. A weak correlation, near the limit of significance, also was observed for BLT and CT for rings 1 and 3 (Table 3). All other layers showed no significant correlation.

Discussion

Corneal pathologies, such as ectatic diseases, often manifest themselves in thickness changes of corneal layers.[18,30] Thus,

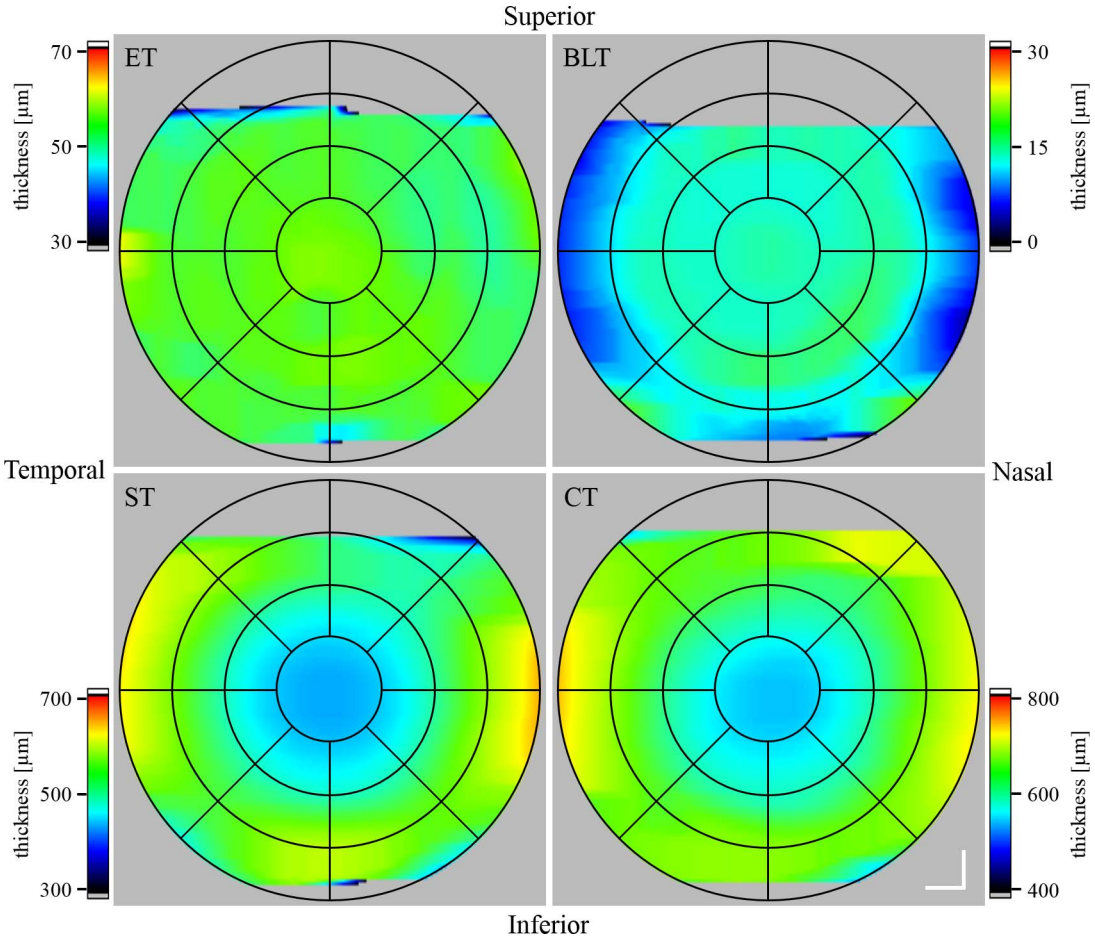

Figure 5. Representative thickness maps of ET, BLT, ST, and CT obtained in the right eye of a healthy volunteer with the sector-map superimposed. *Scale bars*: 1 mm.

for early diagnosis and screening purposes, precise knowledge of thickness parameters is crucial.[31]

We demonstrated a novel approach for segmentation and mapping of corneal layers by combining two well-established approaches. First, we used conical scanning, which improves the SNR in the corneal periphery, and second, we used the additional contrast provided by PS-OCT for the segmentation of corneal layers, especially Bowman's layer, which has proven to be difficult in the past.

An advantage compared to some commercial systems, which acquire few radial scans for evaluation, is that we acquire whole 3D data sets using raster scanning and, thus, are not susceptible to missing small corneal defects, especially in

Table 2. Correlation Data Between Right and Left Eyes of the Same Individual Considering All 20 Eye Pairs

	Correlation Between Right and Left Eyes			
	ET	**BLT**	**ST**	**CT**
Center				
r	0.97	0.90	0.97	0.96
P	<0.001	<0.001	<0.001	<0.001
First ring				
r	0.79	0.83	0.89	0.84
P	<0.001	0.001	<0.001	<0.001
Second ring				
r	0.54	0.61	0.85	0.85
P	0.016	0.005	<0.001	<0.001
Third ring				
r	0.47	0.44	0.42	0.48
P	0.039	0.057	0.073	0.036

Pearson correlation coefficient *r* and the corresponding *P* value between right and left eyes, for the central sector and for three concentric rings of each layer.

Table 3. Correlation Data Between Corneal Layers

	Correlation Between Corneal Layers			
	ET-BLT	**ET-CT**	**BLT-CT**	**ST-CT**
Center				
r	−0.27	−0.07	0.26	0.99
P	0.08	0.67	0.10	<0.001
First ring				
r	−0.14	0.14	0.31	0.98
P	0.37	0.38	0.05	<0.001
Second ring				
r	−0.11	0.12	0.21	0.98
P	0.48	0.43	0.19	<0.001
Third ring				
r	−0.06	0.09	0.32	0.95
P	0.69	0.38	0.04	<0.001

Pearson correlation coefficient *r* and the corresponding *P* value for the central sector and three concentric rings considering all 40 measured eyes.

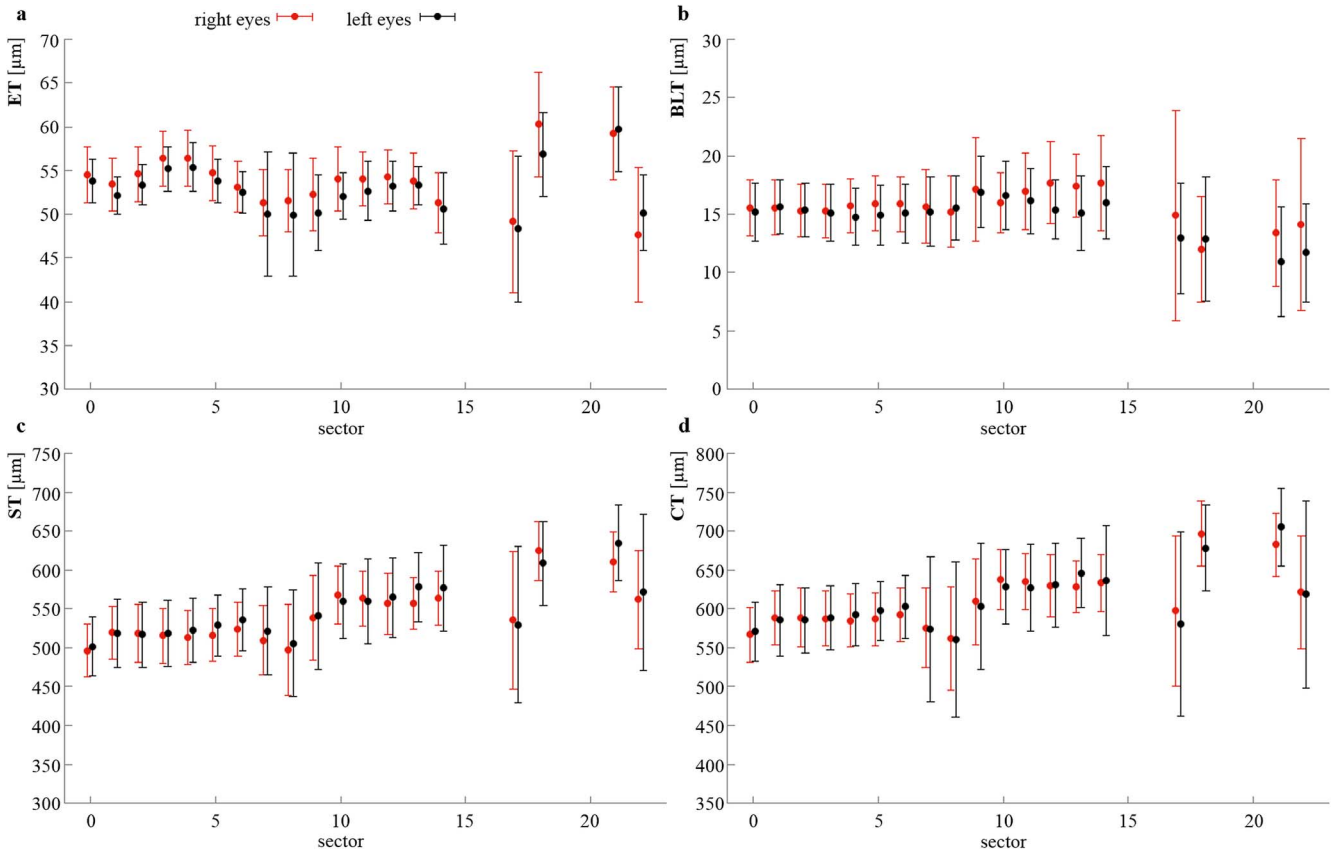

FIGURE 6. Evaluation of corneal layer thicknesses over the entire study group (**a**) ET, (**b**) BLT, (**c**) ST, and (**d**) CT of right (*red*) and left (*black*) eyes for each sector, averaged over all measured eyes. *Error bars*: Variation among subjects (SD).

the corneal periphery.[32] This might be negligible when measuring layer thicknesses in healthy subjects, but can be of great importance for future imaging of pathologic corneas.

A possible drawback of OCT measurements is that motion and blinking artifacts can corrupt the results; however, the short acquisition time of <2 seconds helps to minimize the influence of motion artifacts. Furthermore, axial motion is compensated due to the flattening of the entire data set. Only large lateral motion and blinking cannot be compensated and, therefore, such an invalid data set must be excluded from evaluation. Faster acquisition and the use of a Lissajous scanning pattern[33] might allow for further reduction and compensation of motion artifacts, but would either increase the cost of the system or complicate post-processing.

Previous studies using various imaging modalities, like confocal microscopy,[34] VHF ultrasound,[35] and OCT,[12,15] found ET values varying from approximately 50 to 60 µm and an increase in thickness from superior to inferior, for

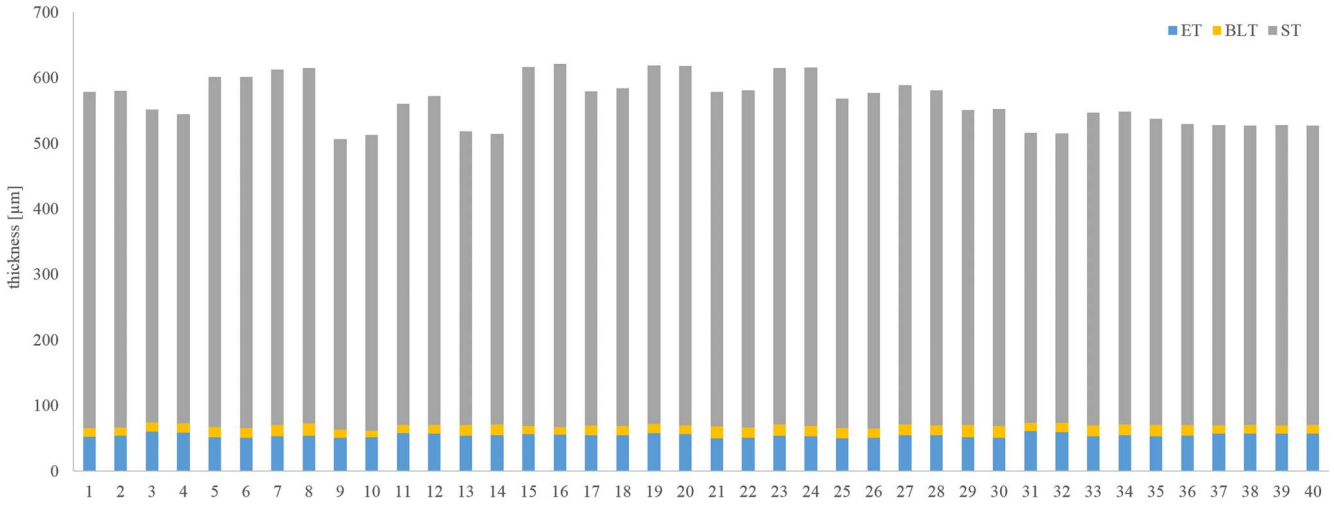

FIGURE 7. Contributions of ET, BLT, and ST to CT of 20 measured eye pairs (odd numbers, right eyes; even numbers, left eyes; adjacent columns are eye pairs, e.g. 1–2, 3–4, and so forth).

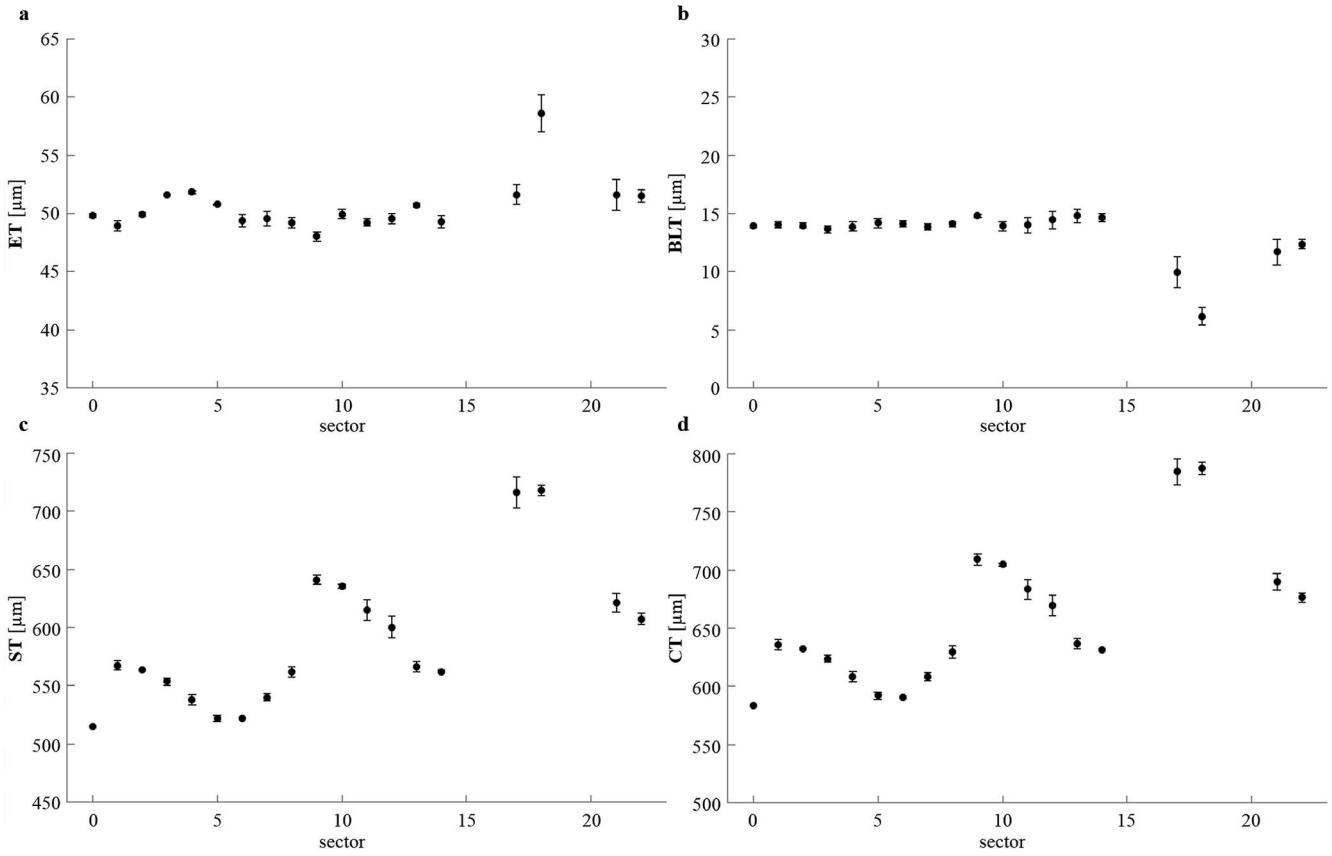

FIGURE 8. Mean ET (**a**), BLT (**b**), ST (**c**), and CT (**d**) for each sector of one representative eye measured four times. *Error bars*: SD between consecutive measurements.

which three possible reasons were described in the literature. First, friction forces due to blinking might ablate the epithelium. These friction forces are thought to be higher in superior regions of the cornea, because the upper eye lid covers more corneal surface than the lower one.[36] Second, the upper eye lid covers at least 2 mm of the superior corneal surface, while the lower one covers less of the inferior cornea. Therefore, the constant pressure applied by the upper eye lid might cause a modification of the epithelium.[37] Third, the pooling of the tear film at the inferior meridian can distort the measured inferior ET.[38] Compared to the studies mentioned previously, we found similar results regarding ET and thickness distribution but were able to do so with a larger FoV of 11 mm diameter. The reproducibility of our ET measurements is comparable to that of commercially-available devices.[15] It was lower in the outmost peripheral sectors, compared to the central sectors, which might be due to small misalignment between consecutive measurements of an eye and segmentation imperfections due to peripheral optical aberrations of the scanning lens. This applies to all segmented layers.

Bowman's layer was described by histology as an approximately 15 µm thick, smooth layer.[2] Only few studies on measuring or even mapping the thickness of Bowman's layer with UHR OCT can be found.[13,16–18] Variations in thickness (from 15[18] to 19[13] µm) and thickness distribution (from uniform central thickness with peripheral increase[16] to the central BLT being highest[13]) can be found comparing the aforementioned studies. We measured an almost uniform BLT with an average of 15.4 ± 2.4 µm at sectors 0 to 8, followed by a slight increase to 16.5 ± 3.2 µm in sectors 9 to 14 and a rapid thinning toward the limbus. Considering an average BLT of 15 µm and the system's axial resolution of 6.3 µm, the reproducibility of 0.3 µm (SD) in the central sector to 2.4 µm (SD) in the outmost ring is quite promising.

The corneal stroma, being the main contributor to the CT and changes thereof, showed an average central thickness of 498.9 ± 36.1 µm and a radial increase to 552.4 ± 20.4 in the outmost peripheral sectors. The measured values of ST are in agreement with the literature.[2,5,19] The reproducibility of ST measurements was 1.0 µm (SD) in the central sector and decreased to 17.4 µm (SD) in the outmost ring, probably for similar reasons as mentioned in the context of ET measurements.

In a further step, we analyzed the previously reported high interocular corneal symmetry[39] for all corneal layers and our study showed significant correlation of all corneal layers of the right and left eyes of the same individual. The correlation decreases toward the periphery, which might be due to the same reason as the lower reproducibility in these areas. Additionally, the rapid thinning and vanishing of Bowman's layer in the two outmost rings also causes segmentation imperfections, especially for calculation of ET and BLT, which contributes to the lower correlation for those layers. Since corneal pathologies can appear unilateral, a comparison of layer thicknesses between the right and left eyes might be beneficial for early diagnosis and potentially be a valuable screening method.[40]

A limitation of this study is that only healthy eyes were included. In a next step, we plan to extend the study to patients with diseases, such as keratoconus, and to analyze if

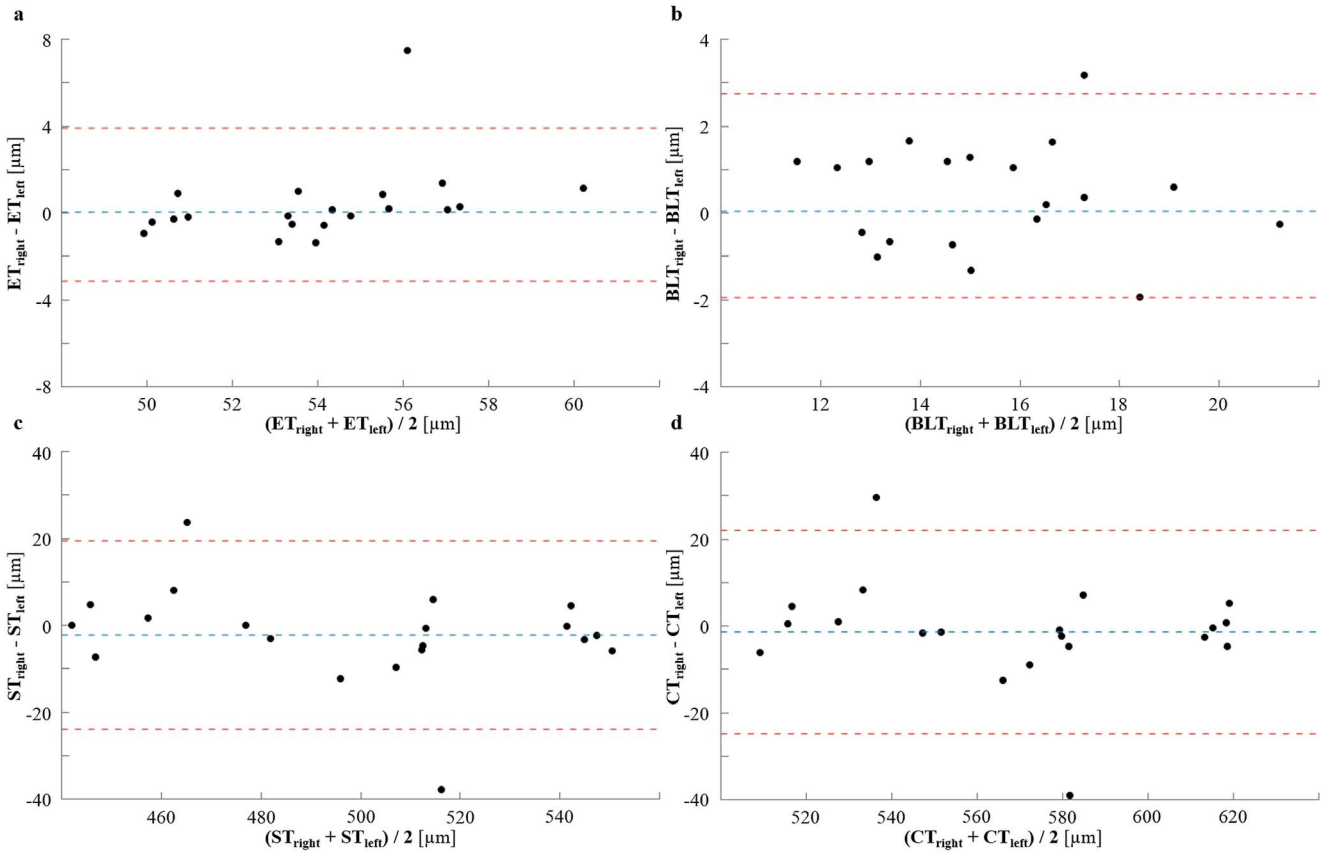

Figure 9. Bland-Altman plot showing the difference between right and left ET (**a**), BLT (**b**), ST (**c**), and CT (**d**) as a function of the mean for the central sector. The mean difference is denoted by *dashed blue lines* and *dashed red lines* denote limits of agreement (mean difference ± 1.96 * SD of difference).

our algorithms also work in corneas with smaller radius of curvature, or if the algorithms need some adaptation.

Acknowledgements

Parts of the results presented in this article have been presented at SPIE Photonics West, BiOS, Ophthalmic Technologies XXVIII (San Francisco, CA, USA, January 2018, program number 10474-8) and at the ARVO 2018 Annual Meeting (Honolulu, HI, USA, April 2018, presentation number 1975).

The authors thank Marco Augustin, Danielle J. Harper, Pablo Eugui, and Antonia Lichtenegger from the Center for Medical Physics and Biomedical Engineering (Medical University of Vienna), and Martin Gröschl from the Institute of Applied Physics (Vienna University of Technology) for their assistance and helpful discussions.

Supported by the Austrian Science Fund (FWF Grant P26553-N20) and the Christian Doppler Laboratory (CDL; OPTIMA).

Disclosure: **F. Beer**, None; **A. Wartak**, None; **N. Pircher**, None; **S. Holzer**, None; **J. Lammer**, None; **G. Schmidinger**, None; **B. Baumann**, None; **M. Pircher**, Canon (F) P; **C. K. Hitzenberger**, Canon (F) P

References

1. Farjo AA, Brumm MV, Soong HK. Corneal anatomy, physiology, and wound healing. In: Yanoff M, Duker JS, eds. *Ophthalmol*. 3rd ed. St Louis, MO: Mosby; 2008:203–208.
2. DelMonte DW, Kim T. Anatomy and physiology of the cornea and related structures. *J Cataract Refract Surg*. 2011;37:588–598.
3. Tavakoli M, Hossain P, Malik RA. Clinical applications of corneal confocal microscopy. *Clin Ophthalmol*. 2008;2:435–445.
4. Reinstein DZ, Yap TE, Archer TJ, Gobbe M, Silverman RH. Comparison of corneal epithelial thickness measurement between Fourier-domain OCT and very high-frequency digital ultrasound. *J Refract Surg*. 2015;31:438–445.
5. Reinstein DZ, Archer TJ, Gobbe M, Silverman RH, Coleman DJ. Stromal thickness in the normal cornea: three-dimensional display with artemis very high-frequency digital ultrasound. *J Refract Surg*. 2009;25:776–786.
6. Ang M, Baskaran M, Werkmeister RM, et al. Anterior segment optical coherence tomography. *Prog Retin Eye Res*. 2018;66:132–156.
7. Huang D, Swanson EA, Lin CP, et al. Optical coherence tomography. *Science*. 1991;254:1178–1181.
8. Fercher AF, Drexler W, Hitzenberger CK, Lasser T. Optical coherence tomography - principles and applications. *Reports Prog Phys*. 2003;66:239–303.
9. Drexler W, Fujimoto JG. *Optical Coherence Tomography: Technology and Applications*. 2nd ed. Springer; 2015.
10. Hitzenberger CK, Drexler W, Fercher AF. Measurement of corneal thickness by laser doppler interferometry. *Invest Ophthalmol Vis Sci*. 1992;33:98–103.
11. Hitzenberger CK. Measurement of corneal thickness by low-coherence interferometry. *Appl Opt*. 1992;31:6637–6642.
12. Pircher N, Schwarzhans F, Holzer S, et al. Distinguishing keratoconic eyes and healthy eyes using ultrahigh-resolution (UHR)-OCT based corneal epithelium thickness mapping. *Am J Ophthalmol*. 2018:47–54.

13. Schmoll T, Unterhuber A, Kolbitsch C, Le T, Stingl A, Leitgeb R. Precise thickness measurements of Bowman's layer, epithelium, and tear film. *Optom Vis Sci*. 2012;89:E795–E802.
14. Li Y, Tan O, Brass R, Weiss JL, Huang D. Corneal epithelial thickness mapping by fourier-domain optical coherence tomography in normal and keratoconic eyes. *Ophthalmology*. 2012;119:2425–2433.
15. Hashmani N, Hashmani S, Saad CM. Wide corneal epithelial mapping using an optical coherence tomography. *Invest Ophthalmol Vis Sci*. 2018;59:1652–1658.
16. Tao A, Wang J, Chen Q, et al. Topographic thickness of Bowman's layer determined by ultra-high resolution spectral domain-optical coherence tomography. *Invest Ophthalmol Vis Sci*. 2011;52:3901–3907.
17. Lian Y, Shen M, Jiang J, et al. Vertical and horizontal thickness profiles of the corneal epithelium and Bowman's layer after orthokeratology. *Invest Ophthalmol Vis Sci*. 2013;54:691–696.
18. Abou Shousha M, Perez VL, Fraga Santini Canto AP, et al. The use of Bowman's layer vertical topographic thickness map in the diagnosis of keratoconus. *Ophthalmology*. 2014;121:988–993.
19. Patel SV, McLaren JW, Hodge DO, Bourne WM. Normal human keratocyte density and corneal thickness measurement by using confocal microscopy in vivo. *Invest Ophthalmol Vis Sci*. 2001;42:333–339.
20. Podoleanu A, Charalambous I, Plesea L, Dogariu A, Rosen R. Correction of distortions in optical coherence tomography imaging of the eye. *Phys Med Biol*. 2004;49:1277–1294.
21. Beer F, Wartak A, Haindl R, et al. Conical scan pattern for enhanced visualization of the human cornea using polarization-sensitive OCT. *Biomed Opt Express*. 2017;8:2906–2923.
22. Pircher M, Hitzenberger CK, Schmidt-Erfurth U. Polarization sensitive optical coherence tomography in the human eye. *Prog Retin Eye Res*. 2011;30:431–451.
23. de Boer JF, Hitzenberger CK, Yasuno Y. Polarization sensitive optical coherence tomography – a review [Invited]. *Biomed Opt Express*. 2017;8:1838–1873.
24. Götzinger E, Pircher M, Sticker M, Fercher AF, Hitzenberger CK. Measurement and imaging of birefringent properties of the human cornea with phase-resolved, polarization-sensitive optical coherence tomography. *J Biomed Opt*. 2004;9:94–102.
25. Götzinger E, Pircher M, Dejaco-Ruhswurm I, Kaminski S, Skorpik C, Hitzenberger CK. Imaging of birefringent properties of keratoconus corneas hy polarization-sensitive optical coherence tomography. *Invest Ophthalmol Vis Sci*. 2007;48:3551–3558.
26. Fukuda S, Yamanari M, Lim Y, et al. Keratoconus diagnosis using anterior segment polarization-sensitive optical coherence tomography. *Invest Ophthalmol Vis Sci*. 2013;54:1384–1391.
27. Pircher M, Goetzinger E, Leitgeb RA, Sattmann H, Hitzenberger CK. Ultrahigh-resolution polarization-sensitive optical coherence tomography. *Coherence Domain Opt Methods Opt Coherence Tomogr Biomed IX*. 2005;5690:257–262.
28. Trasischker W, Zotter S, Torzicky T, et al. Single input state polarization sensitive swept source optical coherence tomography based on an all single mode fiber interferometer. *Biomed Opt Express*. 2014;5:2798–2809.
29. International Electrotechnical Commission. Safety of laser products - part 1: equipment classification and requirements (IEC 60825-1:2007). *Int Stand*. 2014;05:1–13.
30. Kanellopoulos AJ, Asimellis G. Reply: in vivo 3-dimensional corneal epithelial thickness mapping as an indicator of dry eye: Preliminary clinical assessment. *Am J Ophthalmol*. 2014;157:1116–1117.
31. Reinstein DZ, Archer TJ, Gobbe M. Corneal epithelial thickness profile in the diagnosis of keratoconus. *J Refract Surg*. 2009;25:604–610.
32. Yadav R, Kottaiyan R, Ahmad K, Yoon G. Epithelium and Bowman's layer thickness and light scatter in keratoconic cornea evaluated using ultrahigh resolution optical coherence tomography. *J Biomed Opt*. 2012;17:116010.
33. Chen Y, Hong Y-J, Makita S, Yasuno Y. Three-dimensional eye motion correction by Lissajous scan optical coherence tomography. *Biomed Opt Express*. 2017;8:5260–5266.
34. Patel SV, McLaren JW, Hodge DO, Bourne WM. Confocal microscopy in vivo in corneas of long-term contact lens wearers. *Invest Ophthalmol Vis Sci*. 2002;43:995–1003.
35. Reinstein DZ, Archer TJ, Gobbe M, Silverman RH, Coleman DJ. Epithelial thickness in the normal cornea: three-dimensional display with very high frequency ultrasound. *J Refract Surg*. 2008;24:571–581.
36. Reinstein DZ, Silverman RH, Trokel SL, Coleman DJ. Corneal Pachymetric topography. *Ophthalmology*. 1994;101:432–438.
37. Du C, Wang J, Cui L, Shen M, Yuan Y. Vertical and horizontal corneal epithelial thickness profiles determined by ultra-high resolution optical coherence tomography. *Cornea*. 2012;31:1036–1043.
38. King-Smith PE, Fink BA, Fogt N, Nichols KK, Hill RM, Wilson GS. The thickness of the human precorneal tear film: Evidence from reflection spectra. *Invest Ophthalmol Vis Sci*. 2000;41:3348–3359.
39. Myrowitz EH, Kouzis AC, O'Brien TP. High interocular corneal symmetry in average simulated keratometry, central corneal thickness, and posterior elevation. *Optom Vis Sci*. 2005;82:428–431.
40. Bae GH, Kim JR, Kim CH, Lim DH, Chung ES, Chung TY. Corneal topographic and tomographic analysis of fellow eyes in unilateral keratoconus patients using pentacam. *Am J Ophthalmol*. 2014;157:103–109.e1.

Investigative Ophthalmology & Visual Science